Nanoscale Advances

ROYAL SOCIETY OF CHEMISTRY

PAPER

View Article Online
View Journal | View Issue

Cite this: *Nanoscale Adv.*, 2023, **5**, 2487

One-pot synthesis of gamma-graphyne supported Pd nanoparticles with high catalytic activity†

Shan He, ‡ Bin Wu,‡* Ziwei Xia, Panxiang Guo, Yao Li and Shiqiang Song *

As a unique member of the graphyne family, gamma-graphyne (γ-graphyne) is a novel kind of 2D carbon allotrope with potential high carrier mobility and large surface area. It remains a great challenge to synthesize graphynes with targeted topologies and good performance. Herein, a novel one-pot method was applied to the synthesis of γ-graphyne using hexabromobenzene and acetylenedicarboxylic acid *via* a Pd-catalyzed decarboxylative coupling reaction, which is easy to perform with mild reaction conditions, facilitating the possibility of mass production. As a result, the synthesized γ-graphyne reveals a two-dimensional γ-graphyne structure consisting of 1 : 1 sp/sp^2 hybridized carbon atoms. Furthermore, γ-graphyne as a carrier for Pd (Pd/γ-graphyne) displayed a superior catalytic activity for the reduction of 4-nitrophenol with a short reaction time and high yields, even in aqueous media under aerobic conditions. Compared with Pd/GO, Pd/HGO, Pd/CNT, and commercial Pd/C, Pd/γ-graphyne showed more excellent catalytic performance with lower palladium loadings. Thus we expect that the novel approach for the synthesis of γ-graphyne will boost research on the design and application of graphyne-type functional materials for catalysis.

Received 13th February 2023
Accepted 20th March 2023

DOI: 10.1039/d3na00096f

rsc.li/nanoscale-advances

1. Introduction

Carbon nanomaterials, such as fullerenes, carbon nanotubes, graphene, *etc.*, have received much attention due to their special structure and physicochemical properties in many fields.[1,2] To demonstrate their performance, a large batch of carbon nanomaterials with superior performance have been developed by precisely controlled research on material structure design, synthesis methods and application modes. From the structural perspective, most of their frameworks are formed from sp^2 or sp^3 hybridized carbon atoms, however, sp hybridization in the framework could significantly affect their properties. Therefore, the preparation of carbon isomers with unique structures has aroused the interest of researchers and remains a challenge.

The graphyne family (GYs), composed of ethynyl units and aromatic moiety rings, is a class of emerging carbon nanomaterials with highly sp hybridized characteristics.[3] According to the number of ethynyl units between two neighboring aromatic rings, GYs can be divided into graphyne (GY), graphdiyne (GDY), graphtriyne (GTY), *etc.*[4] In 1987, Baughman *et al.*[5] predicted that GYs would be a series of stable crystalline carbon isomers with wide face spacing, excellent chemical stability, special electronic structure, *etc.* Among them, the structural features and basic physical properties including expanded in-plane pores, regular nanostructuring, and good transporting properties make GDY a promising candidate for an electrode material in energy-storage devices.[6] In 2010, GDY was first synthesized on copper foil by cross-coupling reaction using hexaethylbenzene.[7] To date, GYs and their derivatives have been continuously synthesized and play an important role in the fields of energy,[8–11] catalysis,[12–15] photovoltaics,[16] medicine,[17,18] *etc.*

γ-Graphyne is one member of GYs, and its structure can be regarded as two aromatic rings connected by an acetylene bond.[19] Numerous theoretical studies are confirming the excellent performance of γ-graphyne in various fields due to its exceptional strength, moderate-band-gap semiconductivity, high thermal conductivity, ultrafast charge carrier mobility comparable to that of graphene and so on.[20,21] Many approaches have been adopted to prepare γ-graphyne, including mechanical ball milling,[22] and ultrasonic irradiation.[23] However, both mechanical force synthesis and ultrasonic synthesis suffered from complex instruments and equipment as well as the purity of reactants. Recently, alkyne metathesis was used to reversibly cleave and reform the bonds between sp-hybridized carbon atoms as a dynamic covalent synthetic approach to obtain a crystalline γ-graphyne network. For example, Zhang *et al.*[24] employed two types of hexaalkynyl-substituted benzenes as the comonomers to achieve error correction and polymer network growth with periodicity. Rodionov *et al.*[25] reported the synthesis of multilayer γ-graphyne through crystallization-assisted irreversible cross-coupling polymerization. These studies offer the

College of Chemistry and Chemical Engineering, Shanghai University of Engineering Science, Shanghai 201620, People's Republic of China. E-mail: wubinchem@163.com; songchem@126.com

† Electronic supplementary information (ESI) available. See DOI: https://doi.org/10.1039/d3na00096f

‡ These authors contributed equally to this work.

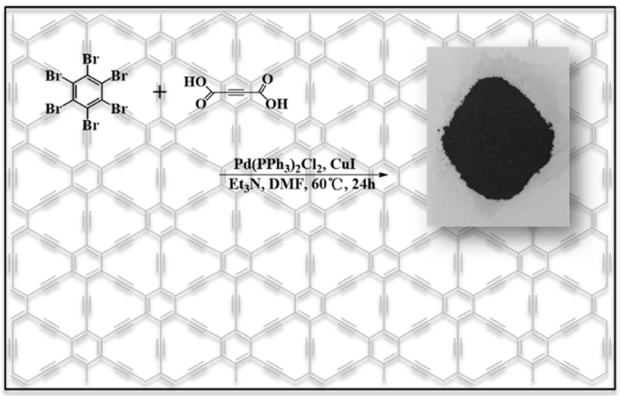

Fig. 1 Schematic outline for the preparation of γ-graphyne.

inspiration to prepare γ-graphyne from different perspectives, however, it remains a great challenge to obtain it by one more economical method.

In this paper, we propose a one-pot method for the synthesis of γ-graphyne using hexabromobenzene and acetylenedicarboxylic acid *via* a Pd-catalyzed decarboxylative coupling reaction, as shown in Fig. 1. The reaction conditions are easy to control and involve low cost without a specific substrate or template. Compared with mechanical ball milling or ultrasonic synthesis methods, it could obtain γ-graphyne in high yield with low equipment requirements, which can effectively meet the requirements of mass production. The as-obtained γ-graphyne showed a two-dimensional structure consisting of 1 : 1 sp and sp^2 hybridized carbon atoms. When ultrafine Pd clusters were deposited onto the γ-graphyne surface, the composite showed superior catalytic activity for the reduction of 4-nitrophenol with a short reaction time and good yields, even in aqueous media under aerobic conditions. γ-Graphyne exhibits a high catalytic performance toward the reduction of 4-nitrophenol compared to Pd/GO, Pd/HGO, Pd/CNT, and commercial Pd/C. Our approach will be significantly beneficial to the design and application of graphyne-type functional materials for catalysis.

2. Results and discussion

As mentioned above, the preparation of γ-graphyne is expected by a mild and convenient method with controllable size and we adopted a one-pot method for the synthesis of γ-graphyne using hexabromobenzene and acetylenedicarboxylic acid *via* a Pd-catalyzed decarboxylative coupling reaction.[26,27] The most likely intermediate process is depicted in Fig. S1.† The polymeric, crystalline and topographical control was managed through adjustable reaction conditions such as time, temperature, reactant ratio, catalyst type, *etc.* As shown in Fig. S2,† the skeleton of the as-prepared sample contains primarily two types of carbon. The peak at 128.3 ppm can be attributed to the sp^2 hybridized carbon atom in the benzene ring (Site 1, Fig. S2†), while the other peak at 78.1 ppm corresponds to the sp hybridized carbon atom in the alkyne chain (Site 2, Fig. S2†). These results indicate that the basic structure of the prepared sample is compatible with γ-graphyne. In Raman spectra, the sample displays two strong absorption peaks (Fig. S3A†), which are attributed to the D peak at ~1378 cm^{-1} and the G peak at ~1529 cm^{-1}. The analysis shows that the defects and disordered structure of the carbon-containing material lead to the appearance of the D peak. The G peak at 1529 cm^{-1} is due to the primary Raman reflection process of the isotropic stretching of the sp^2 hybridized carbon in the benzene ring. The intensity of the G peak is higher than that of the D peak, indicating an ordered structure with fewer faults. A weak peak Y at 2163 cm^{-1} can also be observed, which is caused by the stretching vibration of the sp-hybridized carbon atoms in the conjugated alkyne bond.[28] In addition, the peak at 1293 cm^{-1} assigned to C–Br stretching vibration disappears while two medium peaks at 1384 and 1578 cm^{-1} that are assigned to aromatic carbon atoms appear (Fig. S3B†). Note that no remarkable peak at 2100–2400 cm^{-1} in the FT-IR spectrum represented zero dipole moment C≡C stretching modes, indicating that most of the C≡C bonds in the product were in a symmetrical state.[29]

The XRD patterns provide crystallization information, as shown in Fig. S4.† Compared with the XRD patterns of the hexabromobenzene precursor and the prepared γ-graphyne, the characteristic peaks of hexabromobenzene have vanished from the patterns after a series of removal methods such as benzene washing. The results demonstrate that the unreacted hexabromobenzene has been completely removed and the synthesized γ-graphyne has high crystallinity. γ-Graphyne showed two main peaks at 22.6° and 40.5°, corresponding to the crystal plane of γ-graphyne (002), and the peak of Pd respectively. From the XRD pattern, we can also observe some faint diffraction peaks, confirming that the as-prepared γ-graphyne has a certain content of carbon with a regular graphitization structure.[30] Furthermore, according to the Bragg Equation, the spacing of carbon layers can be calculated as 0.39 nm, suggesting the presence of curved graphene sheets.

EDX was used to investigate the elemental composition of the synthesized γ-graphyne (Fig. S5†). In the γ-graphyne structure, the theoretical ratio of carbon to oxygen is 84.97 and 11.92%, which was similar to that obtained by EDX. EDX mapping further revealed a homogenous distribution of C and O elements (Fig. S6†). As shown in Fig. 2, the peaks at 284.8 and 532 eV were attributed to the C1s and O1s, respectively. The high-resolution XPS spectra of C1s were corrected with Shirley background and fitted with Lorentz and Gaussian functions. The C1s peak was mainly composed of four subpeaks located around 284.5, 285.2, 286.9 and 288.5 eV, which corresponded to C=C(sp^2), C≡C(sp), C–O(sp), and C=O(sp^2), respectively.[31] Among them, the C–O and C=O bonds are due to surface-adsorbed air and certain terminal alkyne oxidation.[32] Both the Raman and XPS reveal the presence of sp and sp^2 hybridized carbon atoms with the area ratio of sp/sp^2 hybridized carbon atoms being 1 : 1, which is compatible with the structure of γ-graphyne. Hence it can be inferred that the sp^2 hybridized carbon atoms in the benzene ring are interconnected through the sp hybridized carbon atoms in acetylene, where the sp and sp^2 hybridized carbons have a high degree of symmetry. These

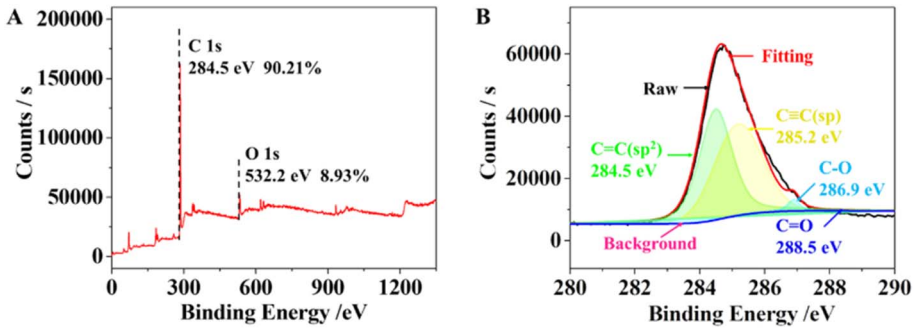

Fig. 2 XPS spectra of γ-graphyne (A) survey scan, and (B) narrow scan for element C.

stable structural characteristics are similar to γ-graphyne. Additionally, the copper and palladium contents were also measured by ICP-MS as 0.03 and 2.75%, respectively. It can be concluded that the copper element has been washed away, but a small amount of palladium is left after the acid-base washing.

The as-prepared samples were characterized morphologically and microstructurally by using SEM and TEM. As shown in Fig. 3, γ-graphyne displays a nanoscale lamellar structure, typical pleated layer morphology and typical 2D structural features. Fig. 4 shows the typical AFM image, indicating that the thickness of graphdiyne films is in the range of 1–2 nm, which is coincident with the TEM observation. The folded structure may be caused by the chemical bonding diversity of carbon forming 2–5 layers approximately according to the above-measured lattice spacing.

To explore the electronic properties of γ-graphyne, valence and conduction band-edge positions of γ-graphyne were obtained from ultraviolet photoelectron spectra (UPS, Fig. S7A†) and UV diffuse reflectance spectra (UV-Vis DRS, Fig. S7B†). The E_{cutoff} value of graphyne obtained by UPS is 13.84 eV. The work function (Φ) was thus calculated with the equation, $\Phi = h\nu - E_{Fermi} + E_{cutoff}$, where $h\nu$, E_{Fermi}, and E_{cutoff} are the photon energy of the excitation light (21.22 eV), the Fermi level edge (calibrated with silver in this case), and the inelastic secondary electron cutoff measured by UPS, respectively. The reduction potential was obtained from the equation,[33] $\Phi/e = E$ (*vs.* SHE) + 4.44 V, where Φ is the work function, and E is the reduction potential *versus* standard hydrogen electrode (SHE). Based on these equations, Φ and E_{vsSHE} were calculated to be 4.29 eV and E_{vsSHE} of −0.15 V for γ-graphyne. The reduction potential of γ-graphyne was estimated to be about −0.15 V *vs.* SHE, which was lower than that of other carbon allotropes such as carbon nanotubes[33] (+0.50 V *vs.* SHE) and graphene oxide[34] (+0.48 V *vs.* SCE), suggesting that γ-graphyne is an excellent reducing agent among carbon materials for electroless deposition of metals. The valence band-edge position of graphyne was estimated to be about 2.09 eV. The conduction band-edge position was obtained by the Mott–Schottky plot according to impedance measurements.[35] And the band gap was calculated to be 2.49 eV based on UV-Vis DRS (Fig. S7C†). The results indicated that γ-graphyne has a natural band gap, in contrast to the zero band gap of graphene.

In addition, we further investigated the pore structure of the sample by nitrogen adsorption/desorption tests (Fig. S8†). γ-Graphyne showed a type IV isotherm for nitrogen adsorption and desorption. The near vertical part of the curve around 1.0 P/P_0 indicates that it has mesoporous properties. The H3-type hysteresis loop at high pressure indicates the presence of mesoporous structure with multilayer adsorption, and also indicates that the sample has a loose accumulation of lamellar particles forming wedge-shaped pores. Meanwhile, the pore size distribution increases from 5 nm to 90 nm, indicating that γ-graphyne has both mesoporous and macroporous structures, which has high material diffusion and mass transfer rate, as well as high specific surface area and many chemical active sites. The mixed pore structures provide some advantages such as "domain-limiting effect". Additionally, the TG-DSC curves showed high thermal stability (up to 200 °C) of γ-graphyne (Fig. S9†).

γ-Graphyne featured a 2D layered structure with remarkable chemical and physical properties, including a large specific surface area and ultra-high carrier mobility, while the presence

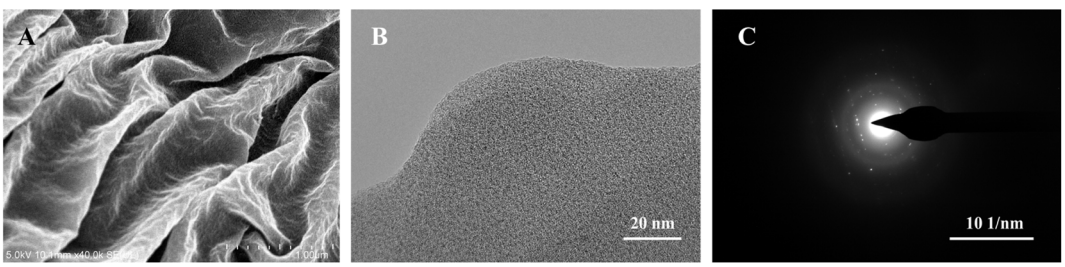

Fig. 3 (A) The SEM image, (B) the TEM image, and (C) the SAED pattern of γ-graphyne.

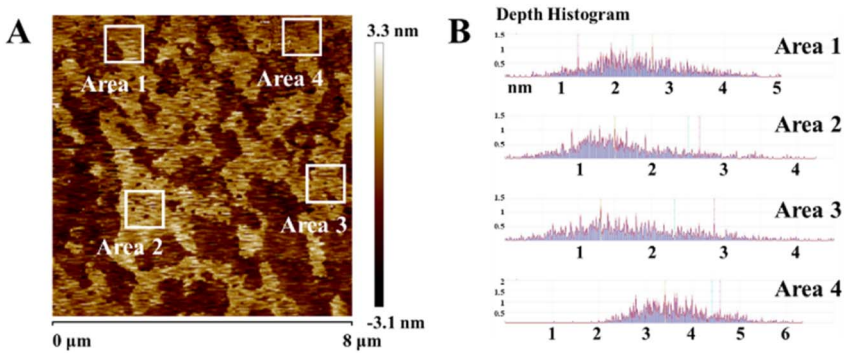

Fig. 4 (A) AFM images of γ-graphyne; (B) the distribution of the γ-graphyne film height marked in (A).

of folded bands makes it extremely ductile. It was found that there are some nanoparticles deposited on parts of the γ-graphyne film (Fig. 5A). The reduction potential of γ-graphyne was estimated to be around −0.15 V *vs.* SHE, which suggests that γ-graphyne was an excellent reducing agent for the electroless deposition of metals from the corresponding metallic ions. As shown in Fig. 5B, the high-resolution transmission electron microscopy (HRTEM) image displays the particle lattice with a planar spacing of 0.222 nm, which is consistent with the (111) lattice spacing of face-centered cubic Pd (0.224 nm). This phenomenon may contribute to the deposition of Pd onto the surface of γ-graphyne driven by the high π-conjugated structure of γ-graphyne that can interact with Pd. In contrast, it provides the possibility for γ-graphyne to be an ideal substrate for a Pd catalyst (Pd/γ-graphyne). More importantly, due to the weak Pd–carrier interactions, the Pd nanoparticles tend to agglomerate and be washed away during the reaction, resulting in a less durable catalyst. However, the Pd nanoparticle content remains 2.92% after various washes owing to the strong interaction between Pd nanoparticles and γ-graphyne that originated from the presence of more active sp hybridized carbon atoms in γ-graphyne. The hybridization allows the in-plane P_x–P_y π/π* orbitals to rotate in any direction perpendicular to the C≡C bond in a specific acetylene ring, and the π/π* orbitals of the C≡C bond may point to the Pd nanoparticles.[36,37] To verify the chemical deposition of Pd on γ-graphyne, we used XPS to demonstrate the presence of Pd particles (Fig. 5C). It showed corresponding peaks at $3d_{5/2}$ and $3d_{3/2}$ energy levels with binding energies of 336.9 and 341.8 eV, respectively, indicating the formation of metallic Pd(0) and likewise confirming the successful deposition of Pd on γ-graphyne during the process.

To prove that Pd/γ-graphyne has high catalytic performance, the reduction of 4-nitrophenol (4-NP) by $NaBH_4$ was used as a model reaction to investigate the synthesized γ-graphyne. As shown in Fig. S10,† a strong absorption peak at 316 nm assigned to 4-NP disappeared, and a new absorption peak at 400 nm appeared after the addition of $NaBH_4$. It indicates the reduction of 4-NP to 4-nitrophenol ions. Meanwhile, the solution color changed from pale yellow to bright yellow.[38,39] When Pd/γ-graphyne was incorporated into the mixture of 4-NP and $NaBH_4$, the absorption peak at 400 nm decreased rapidly, and a new characteristic peak at 300 nm appeared (Fig. S10C†),[40] indicating the reduction of 4-NP and the formation of 4-AP.

Since the concentration of $NaBH_4$ is much larger than that of 4-NP during the reduction, the reaction is considered quasi-primary only concerning 4-NP. The rate of the reaction was determined as shown in the ESI (Fig. S11†). The absorbance is proportional to the concentration of 4-NP in the system, and the value of $\ln(A_t/A_0)$ reflects the value of $\ln(C_t/C_0)$, where C_t and C_0 are the concentrations of 4-NP at moments t and 0, respectively. From the reaction rate equation, $\ln(C_t/C_0) = kt$,[41] the reaction rate constant k can be calculated. To follow the reaction kinetics, the UV-vis spectra of the reaction mixture were monitored periodically. Fig. 6A shows the UV-vis spectra of 4-NP over

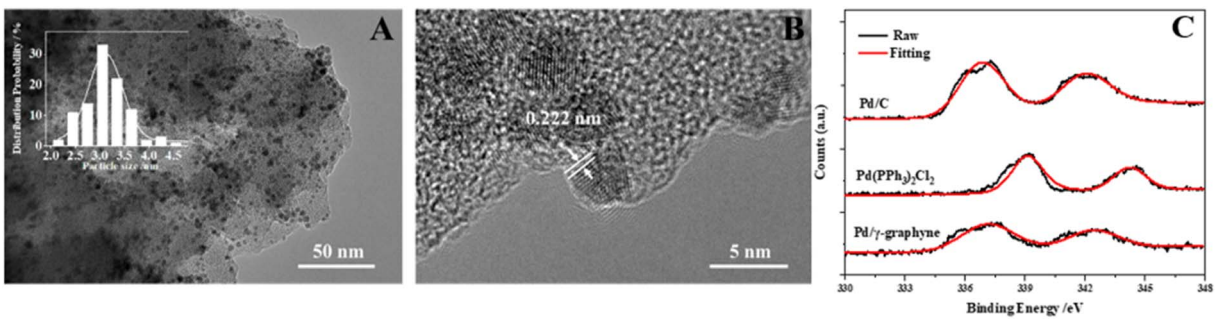

Fig. 5 (A) The TEM and images and particle size distributions(inset); (B) the HR-TEM image of Pd nanoparticle loaded γ-graphyne; (C) XPS high-resolution spectra of Pd3d in Pd/C, $Pd(PPh_3)_2Cl_2$ and Pd/γ-graphyne.

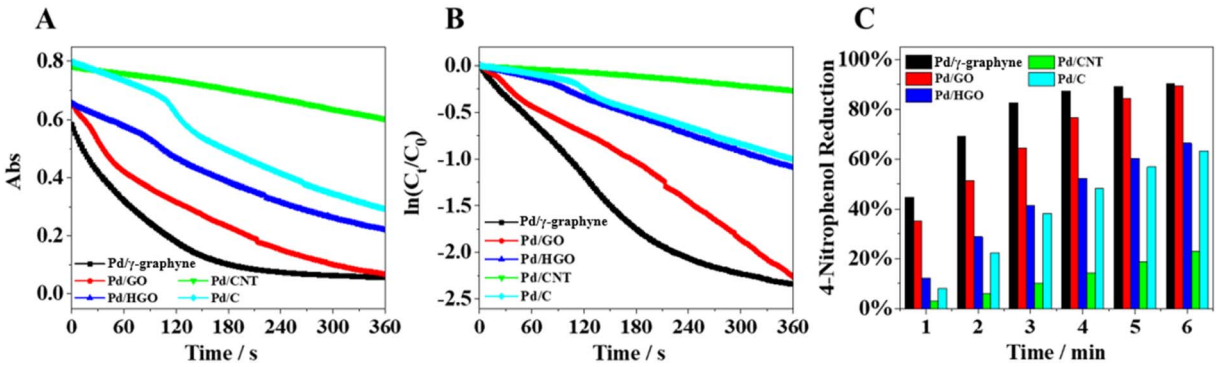

Fig. 6 The reduction of 4-nitrophenol (4-NP) by $NaBH_4$ catalyzed by different methods of Pd/γ-graphyne (black), Pd/GO (red), Pd/HGO (blue), Pd/CNT (green) and commercial Pd/C (cyan). (A) Absorbance (400 nm) *vs.* time (s), (B) $\ln(C_t/C_0)$ as a function of absorbance (400 nm) *vs.* time (s), (C) 4-nitrophenol reduction as a function of absorbance (400 nm) *vs.* time (min).

the Pd/γ-graphyne catalyst during its reduction by $NaBH_4$ as a function of time. The rate constant k was calculated from the slope of the fitted line (Fig. 6B) to be 0.00972 s^{-1}. To further investigate the effect of carrier materials on the catalytic activity of 4-NP reduction, we spontaneously deposited Pd NPs on the surface of other carbon materials by redox reactions between $PdCl^{2-}$ ions and carbon materials, including graphene oxide (GO), reduced graphene oxide (HGO) and carbon nanotubes (CNTs). The catalytic activities of these materials were compared with those of commercial Pd/C and the synthesized Pd/γ-graphyne. The catalytic rate constants of Pd/GO, Pd/HGO, Pd/CNT and commercial Pd/C were measured as 0.00559 s^{-1}, 0.00308 s^{-1}, 0.000567 s^{-1}, and 0.00281 s^{-1}, respectively. By comparison, it can be seen that the Pd particle content of Pd/GO is three times higher than that of the synthesized product, and the rate constant of Pd/γ-graphyne is 1.7-fold higher than that of Pd/GO at the same catalyst mass. The rate constant of the other catalysts is also much lower than that of the synthesized Pd/γ-graphyne under the condition that the Pd particle content is much higher than that of the synthesized Pd/γ-graphyne (Fig. 6C). Therefore, Pd/γ-graphyne has such excellent catalytic performance mainly due to Pd particles deposited on the surface during the synthesis of γ-graphyne, which makes it more dispersive. These results suggest that the smaller Pd clusters and larger conjugated structure are the main reasons for the higher catalytic efficiency of Pd/γ-graphyne in 4-NP reduction compared to Pd/GO, Pd/HGO, Pd/CNT and commercial Pd/C.

3. Conclusions

In summary, we have synthesized γ-graphyne with a few-layered structure by a new and straightforward synthesis method. Raman spectra, XRD, HRTEM, AFM and XPS results confirmed the structure, morphology and components of the as-synthesised product. During the Pd-catalyzed synthesis, Pd is deposited on γ-graphyne to form new highly functional Pd catalysts. Compared with Pd/GO, Pd/HGO, Pd/CNT and commercial Pd/C, Pd/γ-graphyne exhibits higher catalytic activity for the reduction of 4-NP, which is attributed to the synergistic impact of Pd nanoparticles and γ-graphyne. This means that γ-graphyne could be an outstanding electronic transporting medium for catalysts, batteries and other applications. The understanding of the structure–property relationships at the nano level would drive many physical inquiries and could have the potential to positively impact both materials and catalysis science.

Conflicts of interest

There are no conflicts to declare.

Acknowledgements

We acknowledge financial support from the Opening Foundation of the Key Laboratory of Resource Chemistry of the Ministry of Education (Shanghai Normal University).

References

1 A. Hirsch, *Nat. Mater.*, 2010, **9**, 868–871.
2 S. Song, C. Zhang, W. Li, J. Wang, P. Rao, J. Wang, T. Li and Y. Zhang, *Nano Energy*, 2022, **100**, 107513.
3 M. Liu and Y. Li, *Acta Phys.-Chim. Sin.*, 2018, **34**(9), 959–960.
4 C. Huang, Y. Li, N. Wang, Y. Xue, Z. Zuo, H. Liu and Y. Li, *Chem. Rev.*, 2018, **118**, 7744–7803.
5 R. H. Baughman, H. Eckhardt and M. Kertesz, *J. Chem. Phys.*, 1987, **87**, 6687–6699.
6 N. Wang, J. He, K. Wang, Y. Zhao, T. Jiu, C. Huang and Y. Li, *Adv. Mater.*, 2019, **31**, 1803202.
7 G. Li, Y. Li, H. Liu, Y. Guo, Y. Li and D. Zhu, *Chem. Commun.*, 2010, **46**, 3256–3258.
8 Y. Xue, Y. Li, J. Zhang, Z. Liu and Y. Zhao, *Sci. China: Chem.*, 2018, **61**, 765–786.
9 J. Li, T. Jiu, S. Chen, L. Liu, Q. Yao, F. Bi, C. Zhao, Z. Wang, M. Zhao, G. Zhang, Y. Xue, F. Lu and Y. Li, *Nano Lett.*, 2018, **18**, 6941–6947.
10 F. Wang, Z. Zuo, L. Li, F. He and Y. Li, *Nano Energy*, 2020, **68**, 2211–2855.

11 S. Zhang, H. Si, W. Fan, M. Shi, M. Li, C. Xu, Z. Zhang, Q. Liao, A. Sattar, Z. Kang and Y. Zhang, *Angew. Chem., Int. Ed. Engl.*, 2020, **59**, 11573–11582.
12 B. Li, C. Lai, M. Zhang, G. Zeng, S. Liu, D. Huang, L. Qin, X. Liu, H. Yi, F. Xu, N. An and L. Chen, *Adv. Energy Mater.*, 2020, **10**, 2000177.
13 M. Sun, T. Wu, Y. Xue, A. W. Dougherty, B. Huang, Y. Li and C.-H. Yan, *Nano Energy*, 2019, **62**, 754–763.
14 J. Zhang and X. Feng, *Joule*, 2018, **2**, 1396–1398.
15 J. Lee, Y. Li, J. Tang and X. Cui, *Acta Phys.-Chim. Sin.*, 2018, **34**, 1080–1087.
16 Y. Zhang, P. Huang, J. Guo, R. Shi, W. Huang, Z. Shi, L. Wu, F. Zhang, L. Gao, C. Li, X. Zhang, J. Xu and H. Zhang, *Adv. Mater.*, 2020, **32**, e2001082.
17 J. Liu, C. Chen and Y. Zhao, *Adv. Mater.*, 2019, **31**, e1804386.
18 W. Jiang, Z. Zhang, Q. Wang, J. Dou, Y. Zhao, Y. Ma, H. Liu, H. Xu and Y. Wang, *Nano Lett.*, 2019, **19**, 4060–4067.
19 A. R. Puigdollers, G. Alonso and P. Gamallo, *Carbon*, 2016, **96**, 879–887.
20 T. He, Y. Kong, A. R. Puente Santiago, M. A. Ahsan, H. Pan and A. Du, *Mater. Chem. Front.*, 2021, **5**, 6392–6412.
21 F. Yao, W. Wang, H. Shi, Z. Xu, M. Zeng, Y. Hu, L. Liu and X. Ji, *ACS Catal.*, 2021, **11**, 14122–14147.
22 Q. Li, Y. Li, Y. Chen, L. Wu, C. Yang and X. Cui, *Carbon*, 2018, **136**, 248–254.
23 W. Ding, M. Sun, Z. Zhang, X. Lin and B. Gao, *Ultrason. Sonochem.*, 2020, **61**, 104850.
24 Y. Hu, C. Wu, Q. Pan, Y. Jin, R. Lyu, V. Martinez, S. Huang, J. Wu, L. J. Wayment, N. A. Clark, M. B. Raschke, Y. Zhao and W. Zhang, *Nat. Synth*, 2022, **1**, 449–454.
25 V. G. Desyatkin, W. B. Martin, A. E. Aliev, N. E. Chapman, A. F. Fonseca, D. S. Galvão, E. R. Miller, K. H. Stone, Z. Wang, D. Zakhidov, F. T. Limpoco, S. R. Almahdali, S. M. Parker, R. H. Baughman and V. O. Rodionov, *J. Am. Chem. Soc.*, 2022, **144**, 17999–18008.
26 J. Moon, M. Jang and S. Lee, *J. Org. Chem.*, 2009, **74**, 1403–1406.
27 K. Park, G. Bae, J. Moon, J. Choe, K. H. Song and S. Lee, *J. Org. Chem.*, 2010, **75**, 6244–6251.
28 R. Liu, X. Gao, J. Zhou, H. Xu, Z. Li, S. Zhang, Z. Xie, J. Zhang and Z. Liu, *Adv. Mater.*, 2017, **29**, 1604665.
29 B. Wu, M. Li, S. Xiao, Y. Qu, X. Qiu, T. Liu, F. Tian, H. Li and S. Xiao, *Nanoscale*, 2017, **9**, 11939–11943.
30 Y. Li, Q. Liu, W. Li, H. Meng, Y. Lu and C. Li, *ACS Appl. Mater. Interfaces*, 2017, **9**, 3895–3901.
31 A. C. Ferrari, J. C. Meyer, V. Scardaci, C. Casiraghi, M. Lazzeri, F. Mauri, S. Piscanec, D. Jiang, K. S. Novoselov, S. Roth and A. K. Geim, *Phys. Rev. Lett.*, 2006, **97**, 187401.
32 J. Zhou, X. Gao, R. Liu, Z. Xie, J. Yang, S. Zhang, G. Zhang, H. Liu, Y. Li, J. Zhang and Z. Liu, *J. Am. Chem. Soc.*, 2015, **137**, 7596–7599.
33 H. C. Choi, M. Shim, S. Bangsaruntip and H. Dai, *J. Am. Chem. Soc.*, 2002, **124**, 9058–9059.
34 X. Chen, G. Wu, J. Chen, X. Chen, Z. Xie and X. Wang, *J. Am. Chem. Soc.*, 2011, **133**, 3693–3695.
35 L. Liao, Q. Zhang, Z. Su, Z. Zhao, Y. Wang, Y. Li, X. Lu, D. Wei, G. Feng, Q. Yu, X. Cai, J. Zhao, Z. Ren, H. Fang, F. Robles-Hernandez, S. Baldelli and J. Bao, *Nat. Nanotechnol.*, 2014, **9**, 69–73.
36 D. W. Ma, T. Li, Q. Wang, G. Yang, C. He, B. Ma and Z. Lu, *Carbon*, 2015, **95**, 756–765.
37 B. Wu, P. Lyu, K. Wang, X. Qiu, T. Liu, F. Zhang, H. Li and S. Xiao, *Res. Chem. Intermed.*, 2018, **44**, 6327–6337.
38 Y. Deng, Z. Sun, J. Liu, C. Liu, J. Wei, W. Li, C. Liu and D. Zhao, *J. Am. Chem. Soc.*, 2010, **132**, 8466–8473.
39 J. Ge, Q. Zhang, T. Zhang and Y. Yin, *Angew. Chem., Int. Ed. Engl.*, 2008, **47**, 8924–8928.
40 Y. Dai, S. Liu and N. Zheng, *J. Am. Chem. Soc.*, 2014, **136**, 5583–5586.
41 K. Halder, G. Bengtson, V. Filiz and V. Abetz, *Appl. Catal., A*, 2018, **555**, 178–188.